Journal of Biomedical Optics

SPIEDigitalLibrary.org/jbo

Long-distance fluorescence lifetime imaging using stimulated emission

Thilo Dellwig
Po-Yen Lin
Fu-Jen Kao

SPIE

Long-distance fluorescence lifetime imaging using stimulated emission

Thilo Dellwig, Po-Yen Lin, and Fu-Jen Kao
National Yang-Ming University, Institute of Biophotonics, Taipei 11221, Taiwan

Abstract. Long-distance stimulated emission imaging has recently been demonstrated as a novel approach for the characterization and imaging of samples containing fluorescent moieties. We present an extension of this methodology through a pump-probe setup for fluorescence lifetime determination and imaging. We measure fluorescence lifetimes of Rhodamine 6G at different solutions and indocyanine green using long-distance fluorescence lifetime imaging. [DOI: 10.1117/1.JBO.17.1.011009]

Keywords: biophotonics; fluorescence; imaging; laser applications.

Paper 11278SS received Jun. 2, 2011; revised manuscript received Oct. 8, 2011; accepted for publication Oct. 11, 2011; published online Feb. 6, 2012.

1 Introduction

Fluorescence (or spontaneous emission), as well as stimulated emission, are widely utilized in optical imaging for biomedical applications. In addition to the use with high-resolution optical microscopy,[1–3] the novel approach of long-distance stimulated emission imaging (LDSEI) has recently been demonstrated by the authors.[4] In this work, we present an extension of the capabilities of LDSEI for the determination of fluorescence lifetimes and the imaging of two-dimensional fluorescence lifetime distributions.

The measurement of fluorescence lifetime has been an effective way to decipher critical molecular dynamics, such as molecular conformation and the changes in nanoenvironment due to solvent and other molecules.[5] It has also been widely used in mapping pertinent cellular parameters, including ion concentration,[6] pH of the environment,[7] and oxygen saturation levels.[8] Current fluorescence lifetime imaging setups, notably fluorescence lifetime imaging microscopy (FLIM),[9,10] are in most cases based upon time-correlated single-photon counting (TCSPC) technology.[11] While TCSPC shows excellent results in terms of acquisition speed and signal-to-noise ratio for fluorescence lifetimes down to 100 ps,[5] lifetime measuring below this value becomes very challenging due to the limitation set forth by high-speed electronics.[12] Electronics with a bandwidth beyond 10 GHz, required for a better temporal resolution, are difficult to realize and become exceedingly complicated and expensive. The method presented here is based upon an optical pump-probe technique and is therefore limited only by the temporal resolution of the light source used, which can be an ultrafast laser with a pulse-width below 100 fs.

In addition, the dark fluorophores with low quantum yield that absorb excitation photons but do not emit sufficient photons due to the dominant non-radiative decay in the energy relaxation processes.[13] Even though TCSPC is the best available method for this domain[14] and significant progress in terms of sensitivity has been made recently by the use of new detectors,[15] the performance of TCSPC for dark or short lifetime (subnanosecond) fluorophores is inherently limited by those dominant relaxation processes. The stimulated emission-based probe-pump technique described here, however, provides the alternative to observe these dark molecules and their corresponding fluorescence lifetimes.[16,17] Hence LDFLI extends the working distance and modalities of fluorescence lifetime imaging, as succinctly discussed in Refs. 18 and 19.

Two of the frequently used fluorophores in biomedical applications are Rhodamine 6G (R6G) and indocyanine green (ICG). R6G is a chemically stable and can be dissolved in a number of solvents to provide a very high fluorescence quantum yield in the visible spectrum.[20] It has been well characterized previously.[21] It is often used as a standard for system calibrations and feasibility demonstrations. We also used R6G for these purposes and, for its very long lifetime of approximately 5 ns, as an "upper limit" fluorescence lifetime example. ICG, on the other hand, is very prominently used in biomedical studies mainly due to its approval by the U.S. Food and Drug Administration for use on human patients. In addition, ICG absorbs and emits light in the near-infrared spectrum, which is favorable for biomedical applications due to the extended penetration depth of infrared light in skin tissue.[22]

These two fluorophores are thus chosen in order to demonstrate the feasibility of the LDFLI technology across a wide range of applications that require different light sources while covering a broad range of fluorescence lifetimes from 5 ns down to 0.5 ns.

2 Experimental Setup

The LDFLI experimental setup is depicted schematically in Fig. 1. The basic working principles and features of the LDSEI setup have been described in detail in Ref. 4. In this work we will only briefly describe the general setup and focus on the changes to the LDSEI setup aimed for lifetime determination and imaging. The most essential modification to the experimental setup is the optical delay stage in the stimulation beam path.

Address all correspondence to: Fu-Jen Kao, Institute of Biophotonics, National Yang-Ming University, Taipei 11221, Taiwan; E-mail: fjkao@ym.edu.tw.

0091-3286/2012/$25.00 © 2012 SPIE

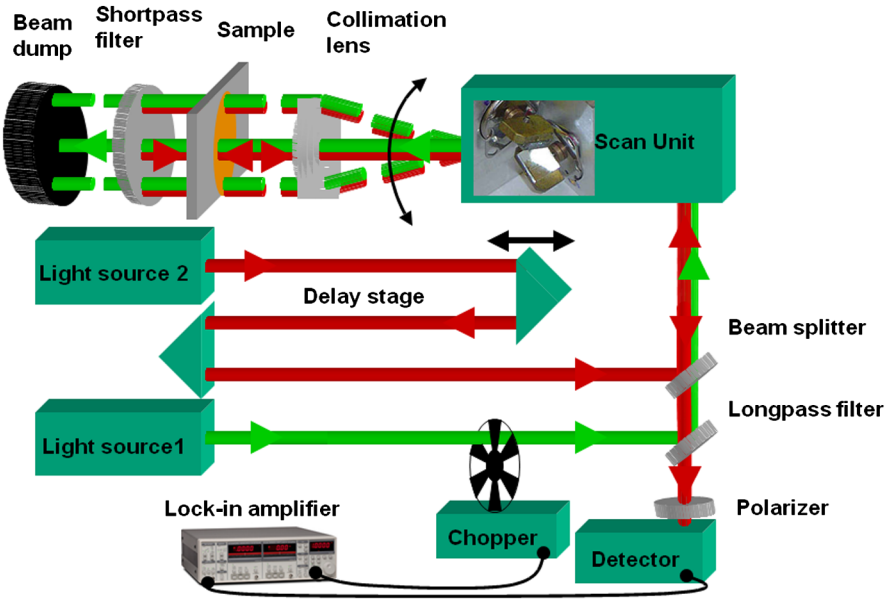

Fig. 1 Experimental setup of the LDFLI. Relative to the LDSEI setup reported in, Ref. 4 the major change is the introduction of the delay stage in the stimulation beam path. The light sources have been chosen according to the fluorescent dye examined.

It has been designed in a way that the length of the stimulation beam pass can be varied by a total of 1 m or 3.3 ns without significant changes in the beam positioning and beam focus at the sample. The advantages of the setup as described in Ref. 4, specifically the use of collimated beams and hence the spatial coherence of the stimulated emission with the stimulation beam, enable long-distance imaging and descanning of the stimulation beam by passing the scan unit twice in opposite directions.

The light sources and detectors utilized were chosen to match the pulse-width and light power best suited for the fluorescence dyes. For R6G, a Fianium broadband fiber laser with a pulse-width of 10 ps, a repetition rate of 2 MHz, and an output power of 20 mW at 530 nm ±20 nm for the excitation beam (light source 1) and 1.2 μW at 570 nm ± 10 nm for the stimulation beam (light source 2) at the sample position, respectively, has been used. The detector was a photomultiplier tube (Hamamatsu H5783 to 04) well suited for the wavelengths utilized.

For ICG detection, we used a coherent MIRA Ti:Sa oscillator with a pulse-width of 250 fs, a repetition rate of 76 MHz, and a wavelength of 790 nm ± 4 nm. A part of the beam was coupled into a photonic crystal fiber (PCF) for continuum generation that covers a broad spectrum and then filtered to create a power of 2 μW at 850 nm ± 10 nm at the sample position as the stimulation beam (light source 2). For the excitation beam (light source one), the remainder of the fundamental 790 nm beam with a laser power of 25 mW at sample position has been used. As most photomultipliers do not have high quantum efficiency in the infrared spectral range, we used a photodiode (Thorlabs DET10A) as the detector instead.

Both laser systems proved to be long-term stable with regards to laser power and beam profile as long as ambient temperature and humidity were kept constant. All dichroic filters in the setup were adopted in accordance with the wavelengths used. The laser beam diameter chosen for the experiments described below was 0.5 mm. This, as opposed to the numerical aperture of the imaging lens, also determines the spatial resolution of the system.[4]

In order to decipher and optimize the signal expected, we compared the laser powers available with similar techniques described in the literature[16,23] and applied the formula derived by Xie et al.[16] to choose the best settings for beam sizes as well as appropriate fluorophore concentrations.

The intensity of the stimulation beams (10^3 W/cm^2) in this study was some magnitudes smaller than the intensities used in stimulated imaging (MW/cm^2)[16] and stimulated emission depletion (STED) microscopy (GW/cm^2).[23] The intensity of excitation beam reaches the order of MW/cm^2 with the chosen beam diameter of 0.5 mm. In combination with a chosen dye concentration yielding 10^{13} molecules in the excited volume, the expected signal strength or depth of modulation, i.e., the ratio of increase in stimulation beam intensity

$$I_{\text{Measured}} = \frac{dI_S}{I_S}, \tag{1}$$

with the stimulation beam intensity I_S when the sample is excited by the excitation beam, for a stimulation beam power below saturation conditions and probing of the sample right after the excitation, is estimated to be 0.6. In order to ensure that the measured signal solely depends upon the remaining population of excited molecules in the sample at a given time delay and independent of the stimulation beam intensity, we used the stimulation beam intensity above the saturation intensity of the given sample (beam power dependencies have been reported in detail in Ref. 4). With that, all molecules in the excited volume are transferred to the excited state, and hence the underlying fluorescence decay curves for the individual delay times are identical. To ensure more complete depletion of the excited fluorophores at the ideal temporal overlap, a relatively high intensity of the stimulation beam, I_S, was chosen. In such a case, I_{Measured} does not reach the estimated maximal value of 0.6. In our experiments the value of 0.2 was reached, within the order of the predicted value and sufficient for a

good signal-to-noise ratio. It shall be pointed out, however, that in order to reach optimum signal-to-noise ratios and to avoid saturation effects, the laser intensities should be chosen according to the geometry and dye concentration of a given sample.

As described above, great care in the experimental setup is given to the high precision and repeatability of the beam positioning and focusing across the entire range of delay stage settings. In order to achieve this goal, a setup including several pinholes for spatial filtering had been chosen. This practice, however, leads to a variation of the stimulation beam intensity at sample position of approximately 25% between the shortest and the longest time delay (3.3 ns). In order to compensate for this variation in intensity, two images have been recorded at each delay stage position, one with the excitation beam enabled and the other without. The measured signal strength, at a given temporal delay Δt, gives

$$I_{\text{Measured}}(\Delta t) = \left[\frac{dI_S(\Delta t)}{I_S(\Delta t)} + 1\right] I_S(\Delta t), \tag{2}$$

where $dI_S(\Delta t)$ is proportional to the number of excited molecules $n_{\text{excited}}(\Delta t)$ and

$$dI_{S,\text{excitation}=0}(\Delta t) = 0 \tag{3}$$

for a disabled excitation beam. The signal of interest

$$\frac{dI_S}{I_S}(\Delta t) = \frac{dI_S(\Delta t)}{I_S(\Delta t)} \tag{4}$$

can hence be estimated as

$$\frac{dI_S}{I_S}(\Delta t) = \frac{I_{\text{Measured}}(\Delta t)}{I_{\text{Measured,excitation}=0}(\Delta t)} - 1. \tag{5}$$

All LDFLI-measured fluorescence decay curves shown below were obtained using the full LDFLI setup including the FV300 scan unit. For R6G no image scans were performed. Instead, the signals were recorded at a fixed position on the sample. The ICG image intensity curves in Fig. 2 were obtained by recording LDFLI images of two different two-dimensional ICG samples using the FV300 scan unit and the Olympus Fluoview software and then determining the average pixel intensity inside the regions of interest marked in Fig. 3 and Fig. 4 of the individual images with the help of ImageJ. The procedure was repeated for different regions of interest, which yielded comparable results. The time delay control between the excitation and stimulation beams for all measurements was realized by mechanically moving a retro-reflector in the delay line of the stimulation beam. To enable the use of a lock-in amplifier for signal discrimination, the excitation beam was modulated at a frequency of 720 Hz using a mechanical chopper. Initial experiments using an electro-optical modulator yielded worse signal-to-noise ratios, even at significantly higher modulation frequencies up to 25 KHz. The degradation of S/N ratio may be attributed to the reduced modulation depth of 10 to 50% relative to the chopper's 100% modulation depth. In addition, the relatively low modulation rate of the chopper compared to

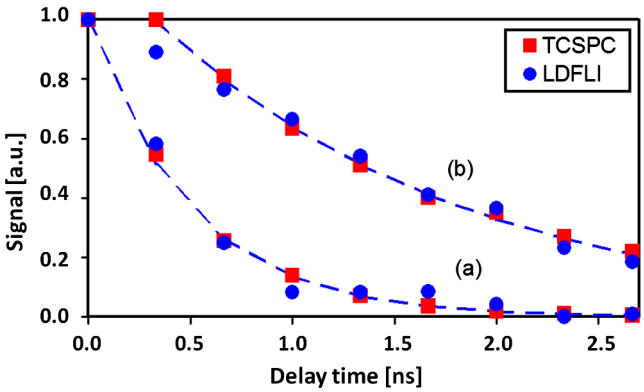

Fig. 2 LDFLI (circles) and TCSPC (squares) signals over time delay for Indocyanine Green dissolved in deionized water, (a) freshly prepared and (b) after 48 h of storage. The data have been derived from the images shown in Fig. 3 and Fig. 4, respectively. The measured fluorescence lifetimes are (a) 0.5 ns and (b) 1.5 ns, respectively.

the high laser repetition rates led to sufficient data point averaging in order to diminish pulse-to-pulse laser power fluctuation effects. The lock-in amplifier signal was either directly recorded or, for the image recording, fed into the scan unit's control computer.

For comparison, the time-correlated single photon counting (TCSPC) measurements were performed using the respective excitation beams for the creation of fluorescence and a PMT-based PicoQuant TimeHarp TCSPC system with an optimum temporal resolution of 37 ps for detection and analysis. The sample position remained unchanged with respect to the LDFLI measurements. The dichroic mirror behind the sample was

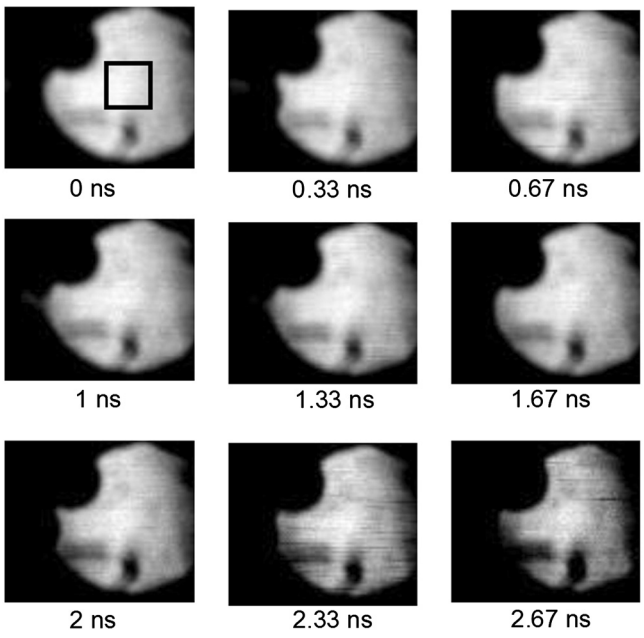

Fig. 3 LDFLI images of a two-dimensional distribution of Indocyanine Green dissolved in deionized water. The numbers below the individual image clips are the respective time delays. The image size is 3 mm × 2.8 mm the pixel size 50 μm × 50 μm. The box in the first images shows the region used for measuring the signal intensity. Note that the image quality suffered during conversion, the data shown in Fig. 2 has been derived from the original images.

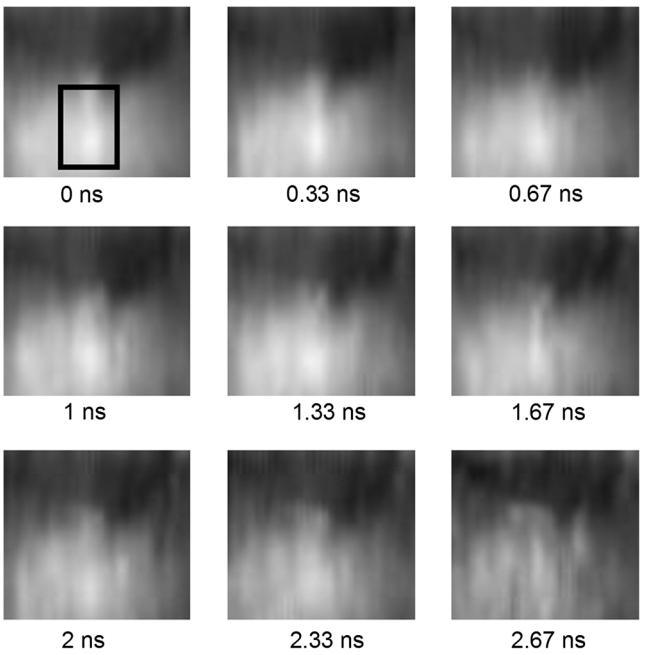

Fig. 4 LDFLI images of a two-dimensional distribution of Indocyanine Green dissolved in deionized water after 48 h of storage at room temperature. The numbers below the individual image clips are the respective time delays. The image size is 3 mm × 2.8 mm, the pixel size 50 $\mu m \times 50\,\mu m$. The box in the first images shows the region used for measuring the signal intensity. Note that the image quality suffered during conversion, the data shown in Fig. 2 has been derived from the original images.

replaced by an appropriate long pass filter mounted before the TCSPC's detector. In order to maintain the identical overall excitation beam power, all optics including the chopper (not used with TCSPC) remained unchanged.

3 Sample Preparation

R6G samples were prepared by dissolving R6G powder in ethanol and glycerol, both HPLC grade, respectively. The concentrations for both solvents were 100 µM. Both solutions are known to be stable with regard to their fluorescence properties over many days under room temperature storage conditions.[24] We hence used the same samples to repeat the measurements using the same samples in a few days. The fluorescence lifetime for R6G reported in literature is 5 ns.[25] For R6G in glycerol, a huge variety of lifetimes has been reported.[26–29]

ICG powder was dissolved in deionized water to a concentration of 65 µM. It is known that this solution is chemically not stable and changes its fluorescence properties over time, depending upon the storage conditions, especially with respect to the intensity of the fluorescence.[30,31] However, changes in fluorescence lifetimes over storage time have, to our knowledge, not yet been reported in literature. We recorded fluorescence lifetimes for freshly prepared ICG samples and for samples stored at room temperature in a light-tight case for 48 h. The fluorescence lifetime of ICG diluted in water reported in the literature is 0.51 ns.[32]

4 Results

Figure 5 shows the results of initial LDFLI measurements and the TCSPC signal measured for R6G dissolved in (a) ethanol and (b) glycerol, respectively. The results demonstrate the lifetime measurement capabilities of LDFLI and determine an "upper limit" for the methodology presented. For both samples, LDFLI and TCSPC measurements are very comparable and can be fitted using the also depicted single exponential decay curves. Being well aware that for this fluorescence lifetime regime TCSPC imaging is a well-established method yielding excellent results for most applications, we nevertheless did not record images in this case, but measured at a static position of the sample. As fluorescence lifetimes above a few nanoseconds are of lesser interest for biomedical applications, we also refrained from measurements above a temporal delay of 3 ns.

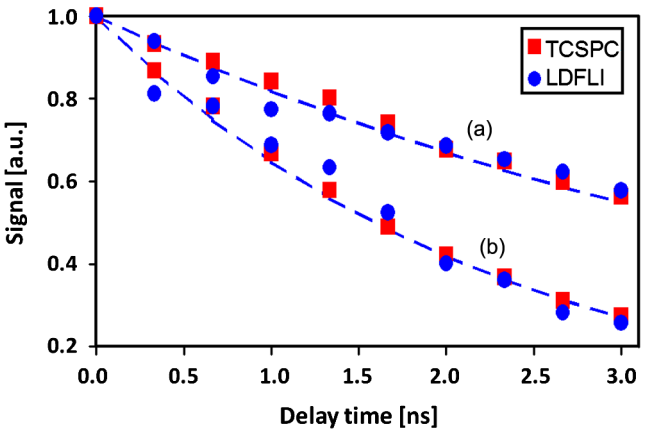

Fig. 5 LDFLI (circles) and TCSPC (squares) signals over time delay for Rhodamine 6G dissolved in (a) ethanol and (b) glycerol. The measured fluorescence lifetimes are (a) 5 ns and (b) 2.3 ns, respectively.

For further measurements and the demonstration of the imaging capabilities of LDFLI, we moved to an ICG sample with a reported fluorescence lifetime that is approximately one order of magnitude shorter than that of R6G. As shown in Figs. 3 and 4, LDFEI produces images recorded at different time delays for a freshly prepared ICG sample (Fig. 3) and for a sample after the ICG had been stored for 48 h in a light-tight case at room temperature (Fig. 4). Only the images recorded with the excitation beam switched on are depicted here, as the signal variation in the reference images recorded without excitation beam cannot clearly be seen after the image conversion necessary for exhibition. In order to determine the fluorescence lifetimes from these images, we integrated the image intensities across the regions of interest depicted in the top left images in Figs. 3 and 4 and applied the theoretical model described above. The signal strength dependence over delay time of the LDFLI measurements, as well as TCSPC reference measurements, are shown in Fig. 2. Again, LDFLI and TCSPC measurements are in very good agreement except for the very beginning of the LDFLI decay curve (b), where saturation effects begin to dominate the signal. This part of the measured curve should therefore not been taken into account for lifetime determination.

We found a significant change of the fluorescence lifetime from 0.5 to 1.5 ns after the storage. This change in ICG lifetime is, to our knowledge, reported for the first time, even though changes in the fluorescence response of ICG as a dependence of storage time have been published earlier.[30,31]

5 Discussion and Outlook

In this work we have shown an extension of LDSEI toward the measurement of fluorescence lifetimes. We demonstrated that our long-distance fluorescence lifetime imaging technique is capable of accurate fluorescence lifetime measurements of fluorophores with lifetimes between 0.5 ns and 5 ns, with absorption and emission spectra in different spectral regions. We also compared these measurements with the well-established method of TCSPC and found the results comparable. Additionally, the capability of LDSEI in imaging two-dimensional fluorescence lifetime distributions is demonstrated. Furthermore, we found a change in fluorescence lifetime of ICG after 48 h of storage at room temperature, which has not been documented before.

These initial results of LDFLI demonstrate the tremendous potential of this novel method, especially toward measuring two-dimensional distributions of short fluorescence lifetime fluorophores. We chose R6G, a fluorophore with a relatively long lifetime of 5 ns, as a first sample in order to provide an "upper limit" for the use of this technique. Additionally, there may be effects attributed to photothermal lens[33] that forms a background of long time constant, which needs to be better discriminated in the coming work. Whereas there are no fundamental limits for the extension of the method toward longer fluorescence lifetimes, the realization of an optical delay stage beyond a length of 1 m presented a technical issue that currently prevents LDFLI from challenging the established TCSPC-based setups. For lifetimes below 1 ns, however, TCSPC-based setups require highly sophisticated and costly components, specifically extremely fast electronics and very careful microwave-compatible connection layouts, whereas the LDFLI setup becomes, due to the decreasing delay stage dimensions, rather competitive. As the critical component for temporal resolution of LDFLI is the light source alone rather than the detector, and the light source can be chosen freely in accordance with the fluorophores under examination, the probing of ultrafast decay processes is now feasible. This can be of use in image-guided surgery[34] or airborne (or perhaps ultimately satellite) biological and environmental monitoring.[35]

Our future work will hence focus on extending the detected lifetime range to significantly shorter fluorescence lifetimes, a domain in which the use of ultrafast pulsed lasers and pump-probe type techniques has the greatest benefits over other methods, as well as on expanding the applied prospects of LDFLI.

One especially interesting application of LDFLI will be the characterization of dark fluorophores in living tissue, such as hemoglobin and cytochromes. Their spontaneous emission is dominated by their fast nonradiative decay processes,[36] and hence very difficult to detect with fluorescence detection methods. The feasibility of imaging such fluorophores for label-free imaging of hemoglobin has been shown by Min et al.[16] The application of LDFLI in this topic will enable the setup of a low-cost, high-throughput characterization apparatus.

Acknowledgments

The authors would like to thank the National Science Council, Taiwan (NSC99-2627-M-010-002, NSC98-2627-M-010-006, NSC97-2112-M-010-002-MY3, and NSC98-2112-M-010-001-MY3), as well as the Ministry of Education, Taiwan under the "Aim for Top University" project for the generous support of the reported work.

References

1. V. Ghukasyan and F.-J. Kao, "Monitoring cellular metabolism with fluorescence lifetime of reduced nicotinamide adenine dinucleotide," *J. Phys. Chem. C* **113**(27), 11532–11540 (2009).
2. F.-J. Kao, "The use of optical parametric oscillator for harmonic generation and two-photon UV fluorescence microscopy," *Micro. Res. and Tech.* **63**(3), 175–181 (2004).
3. V. Ghukasyan et al., "Fluorescence lifetime dynamics of enhanced green fluorescent protein in protein aggregates with expanded polyglutamine," *Biomed J. Opt.* **15**(1), 016008 (2010).
4. T. Dellwig, M. R. Foreman, and F.-J. Kao, "Coherent long-distance signal detection using stimulated emission: a feasibility study," *Chin. Phys. J.* **48**(6), 873–884 (2010).
5. J.R. Lakowicz. *Principles of fluorescence spectroscopy*, 3rd ed., Plenum Press, New York (2006).
6. C. Hille et al., "Two-photon fluorescence lifetime imaging of intracellular chloride in cockroach salivary glands," *Photochem. Photobiol. Sci.* **8**(3), 319–327 (2009).
7. K. M. Hanson et al., "Two-photon fluorescence lifetime imaging of the skin stratum corneum pH gradient," *Biophys. J.* **83**(3), 1682–1690 (2002).
8. H. C. Gerritsen et al., "Fluorescence lifetime imaging of oxygen in cells," *J. Fluoresc.* **7**(1), 11–16 (1997).
9. W. Becker et al., "Fluorescence lifetime imaging by time-correlated single-photon counting," *Microsc. Res. Tech.* **63**(1), 58–66 (2004).
10. Y. Sun, R. N. Day, and A. Periasamy, "Investigating protein-protein interactions in living cells using fluorescence lifetime imaging microscopy," *Nat. Protoc.* **6**(9), 1324–1340 (2011) .
11. D. V. O'Connor and D. Phillips, *Time-correlated single photon counting*, Academic Press, London (1984).
12. W. Becker, *Advanced time-correlated single photon counting techniques*, Springer, Berlin (2005).
13. N. J. Turro, *Modern Molecular Photochemistry*, University Science Books, Mill Valley (1991).
14. E. Gratton et al., "Fluorescence lifetime imaging for the two-photon microscope: time-domain and frequency-domain methods," *Biomed. J. Opt.* **8**(3), 381–390 (2003).
15. W. Becker et al., "FLIM and FCS detection in laser-scanning microscopes: Increased efficiency by GaAsP hybrid detectors," *Microsc. Res. Techn.***74**(9), 804–811 (2010).
16. W. Min et al., "Imaging chromophores with undetectable fluorescence by stimulated emission microscopy," *Nature* **461**(7267), 1105–1109 (2009).
17. C. Y. Dong et al., "Fluorescence lifetime imaging by asynchronous pump-probe microscopy," *Biophys. J.* **69**(6), 2234–2242 (1995).
18. H. Wallrabe and A. Periasamy, "Imaging protein molecules using FRET and FLIM microscopy," *Current Opinion in Biotechnology* **16**(1), 19–27 (2005).
19. E. B. van Munster and T. W. J. Gadella, "Fluorescence lifetime imaging microscopy (FLIM)," *Adv. Biochem. Eng./Biotechnol.* **95**, 1301–1303 (2005).
20. D. Magde, G. E. Rojas, and P. Seybold, "Solvent dependence of the fluorescence lifetimes of xanthene dyes," *Photochem. Photobiol* **70** (5), 737–751 (1999).
21. R. Reisfeld et al., "The spectroscopic behaviour of rhodamine 6G in polar and non-polar solvents and in thin glass and PMMA films," *Chem. Phys. Lett.* **147**(2–3), 142–147 (1988).
22. A. N. Bashkatov et al., "Optical properties of human skin, subcutaneous and mucous tissues in the wavelength range from 400 to 2000 nm," *Phys. J. D: Appl. Phys.* **38**(1), 2543–2555 (2005).
23. B. Harke et al., "Resolution scaling in STED microscopy," *Opt. Express* **16**(6), 4154–4162 (2008).
24. D. Magde, R. Wong, and P. G. Seybold, "Fluorescence quantum yields and their relation to lifetimes of rhodamine 6G and fluorescein in nine solvents: Improved absolute standards for quantum yields," *Photochemistry and Photobiology* **75**(4), 327–334 (2002).

25. A. Penzkofer and W. Leupacher, "Fluorescence behaviour of highly concentrated rhodamine 6G solutions," *Luminisc J.* **37**(2), 61–72 (1987).
26. V. Misra and H. Mishra, "Role of diffusion in excitation energy transfer and migration," *Chem. J. Phys.* **127**(9), 094511 (2007).
27. C. R. Gochanour and M. D. Fayer, "Electronic excited-state transport in random systems. time-resolved fluorescence depolarization measurements," *Phys. J. Chem.* **1081**(85), 1989–1994 (1980).
28. F. Olivini, S. Beretta, and G. Chirico, "Two-photon fluorescence polarization anisotropy decay on highly diluted solutions by phase fluorometry," *Appl. Spectrosc.* **55**(3), 311–317 (2001).
29. J. Hunga, J. Castilloa, and A. Marcano Olaizolab, "Fluorescence spectra of rhodamine 6G for high fluence excitation laser radiation," *Lumin. J.* **101**(4), 263–268 (2003).
30. V. Saxena, M. Sadoqi, and J. Shao, "Degradation kinetics of indocyanine green in aqueous solution," *Pharm. J. Sci.* **92**(10), 2090–2097 (2003).
31. A. Gerega et al., "Wavelength-resolved measurements of fluorescence lifetime of indocyanine green," *Biomed. J. Opt.* **16**(6), 067010 (2011).
32. M. Y. Berezin and S. Achilefu, "Fluorescence lifetime measurements and biological imaging," *Chem. Rev.* **110**(5), 2641–2684 (2010).
33. S. Lu et al., "Label-free imaging of heme proteins with two-photon excited photothermal lens microscopy," *Appl. Phys. Lett.* **96**(11), 113701 (2010).
34. A. M. De Grand and J. V. Frangioni, "An operational near-infrared fluorescence imaging system prototype for large animal surgery," *Technol. Cancer Res. Treat.* **6**(6), 553–562 (2003).
35. M. A. Sundermeyer et al., "Three-dimensional mapping of fluorescent dye using a scanning, depth-resolving airborne lidar," *Atmos. J. Oceanic Technol.* **24**(6), 1050–1065 (2007).
36. N. J. Turro, *Modern Molecular Photochemistry*, University Science Books , Menlo Park, CA1991).